Song et al. Geoscience Letters (2024) 11:34
https://doi.org/10.1186/s40562-024-00350-w

Geoscience Letters

RESEARCH LETTER

Open Access

What caused the record-low frequency of western North Pacific tropical cyclones in autumn 2023?

Jinjie Song[1,2*], Philip J. Klotzbach[3], Na Wei[1] and Yihong Duan[2]

Abstract

September–November (e.g., autumn) 2023 produced the fewest western North Pacific (WNP) tropical cyclones (TCs) since 1951, likely as a joint response to El Niño and a warm phase of the North Pacific Mode (NPM). Decreases in both TC genesis frequency and two genesis potential indices (GPIs) over the western WNP were likely the result of El Niño-induced and warm NPM-induced negative low-level relative vorticity anomalies. Over the eastern WNP, TC genesis and GPI reductions were also associated with vorticity decreases over the eastern WNP, where the TC-suppressing effect of the warm NPM surpassed the TC-favoring effect of El Niño. The changes in vorticity were further linked to anomalous anticyclones centered over the South China Sea and the midlatitude central North Pacific. A linear combination of the responses to El Niño and a warm NPM can explain the changes in TC genesis and low-level circulation over most of the WNP in 2023, except east of 160°E where other climate modes may have played more of a role.

Keywords Tropical cyclone, Western North Pacific, ENSO, North Pacific Mode

Introduction

The western North Pacific (WNP) is the most active basin for tropical cyclone (TC) activity worldwide, producing approximately one-third of global TCs on an annually averaged basis (Maue 2011; Lee et al. 2012). Climatologically, most WNP TCs occur in boreal summer (June–August) and autumn (September–November), accounting for ~43% and ~42% of the annual total number, respectively (Yao et al. 2020). Many studies have examined anomalous boreal summer WNP TC frequency. WNP TC frequency was extremely high in summer 2018, likely driven by the anomalous low-level cyclone that predominated across the WNP that summer, jointly induced by a warm tropical central Pacific and a cold tropical Indian Ocean (Gao et al. 2020; Basconcillo et al. 2021). In contrast, the low WNP TC frequency in summer 2020 was linked to an anomalous low-level anticyclonic circulation over the WNP, mainly because of an anomalously warm tropical Indian Ocean (Wang et al. 2021; Liu et al. 2021). However, few studies have investigated extremes in autumn WNP TC activity. Of note, in autumn 2023, only four TCs formed over the WNP—the fewest in the WNP in autumn since 1951 (Fig. 1a, b). The causes of this remarkably quiet autumn are unknown, and we intend to investigate them further in this manuscript.

Autumn 2023 witnessed the developing phase of a strong El Niño, with a seasonal mean Niño-3 (5°S–5°N, 150°–90°W) sea surface temperature (SST) anomaly (SSTA) exceeding 1.5℃ (Fig. 2a–e). Although El Niño-Southern Oscillation (ENSO) has been shown to be the

*Correspondence:
Jinjie Song
songjinjie@qq.com
[1] Nanjing Joint Institute for Atmospheric Sciences, Chinese Academy of Meteorological Sciences, 8 Yushun Road, Nanjing 210041, China
[2] State Key Laboratory of Severe Weather, Chinese Academy of Meteorological Sciences, Beijing, China
[3] Department of Atmospheric Science, Colorado State University, Fort Collins, CO, USA

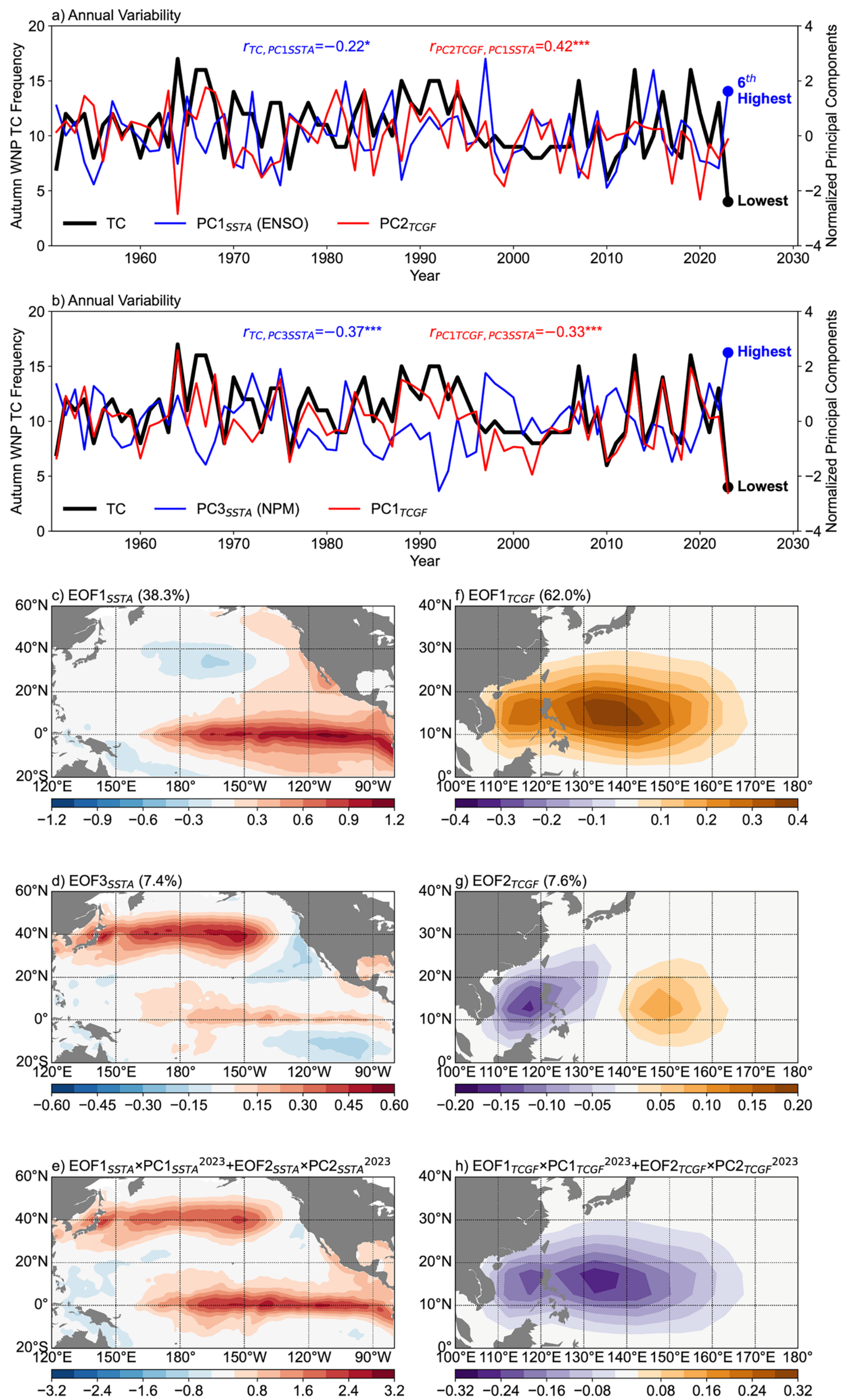

Fig. 1 **a**, **b** Annual variations of WNP TC number, normalized ENSO and NPM indices, as well as the first two principal components of WNP TCGFs in boreal autumn during 1951–2023. The correlation coefficients between two timeseries are given in the panel, while correlations significant at the 0.10, 0.05 and 0.01 levels are marked by "*", "**" and "***", respectively. **c**, **d** The c first and d third leading EOFs of autumn SSTAs over the tropical and North Pacific from 1951 to 2023. The fractions of the SSTA variance explained by these modes are indicated in the titles of the panels. **e** Reconstructed SSTAs based on the first and third EOFs and their corresponding PCs in 2023. **f**, **g** The f first and g second leading EOFs of autumn WNP TCGFs during 1951 to 2023. The fractions of the TCGF variance explained by these modes are indicated in the titles of the panels. **h** Reconstructed TCGF anomalies based on the first and second EOFs and their corresponding PCs in 2023

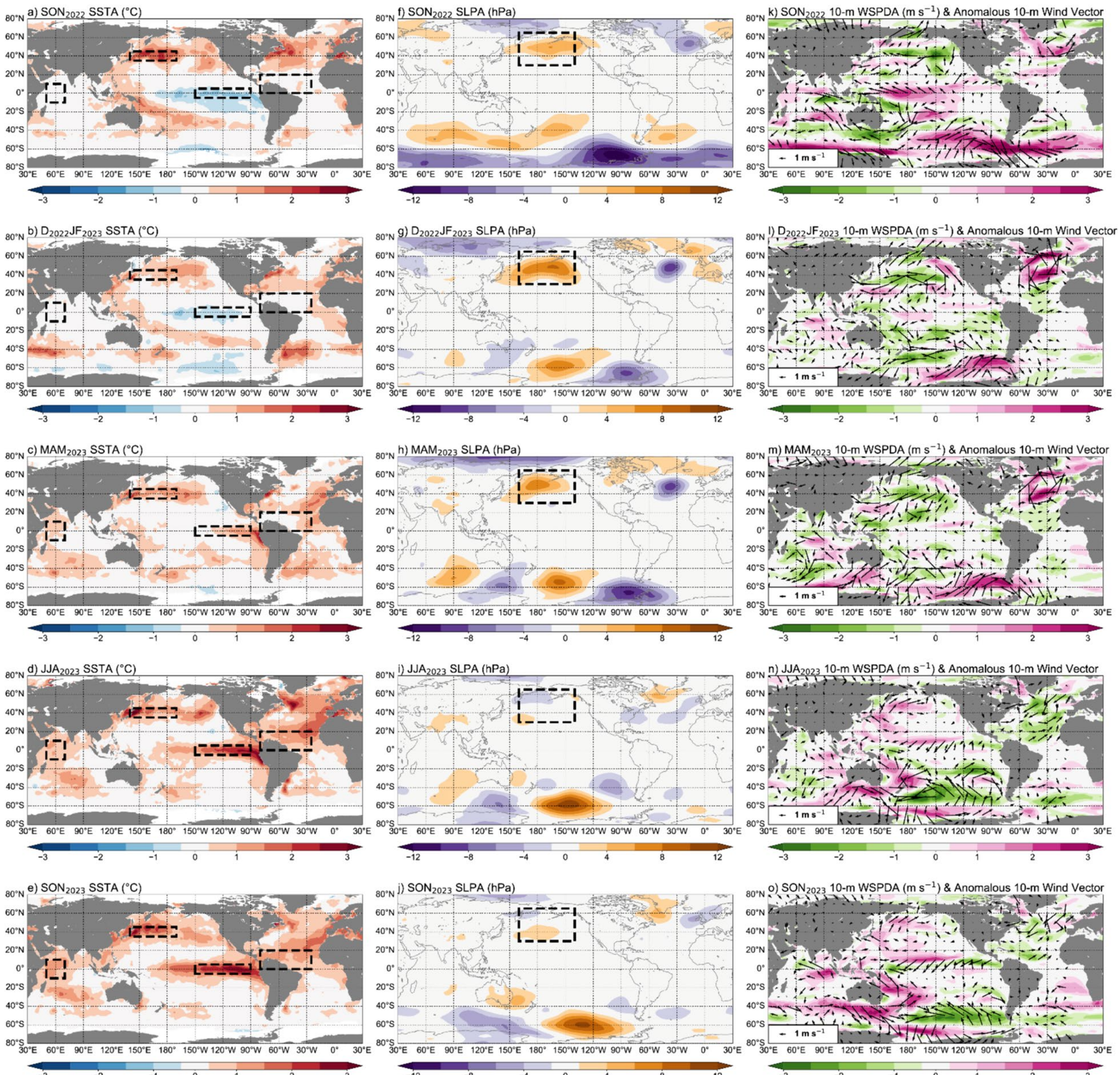

Fig. 2 Seasonal evolution of global **a**–**e** SSTAs, **f**–**j** sea level pressure anomalies and **k**–**o** 10-m wind speed anomalies and anomalous 10-m wind anomalies from autumn 2022 to autumn 2023. Dashed black boxes in a–e refer to the Niño-3 region (5°S–5°N, 150°–90°W), the midlatitude western-to-central North Pacific (35°–45°N, 140°E–170°W), the western equatorial Indian Ocean (10°S–10°N, 50°–70°E,) and the tropical North Atlantic (0°–20°N, 80°–25°W). The dashed black box in f–j denotes the Aleutian Low region (30°–65°N, 160°E–140°W)

most important mode modulating interannual changes in WNP TC activity (Emanuel 2018), there is only a weak correlation between autumn WNP TC numbers and ENSO, regardless of ENSO index considered (Choi et al. 2019). Several other factors have been found to significantly influence autumn WNP TC frequency. Hu et al. (2020) showed that WNP TC frequency from mid-September to mid-October was significantly correlated with the withdrawal date of the South China Sea (SCS) summer monsoon. Fewer (more) TCs formed in early (late) SCS summer monsoon withdrawal years, due to the breakdown (maintenance) of the monsoon trough over the WNP. Zhang et al. (2022) noted that there was a close linkage between September–October WNP TC frequency and Chukchi–Beaufort and Greenland Sea ice variability. Excessive sea ice triggered Rossby wave trains propagating southeastward into the WNP, resulting in an anomalous WNP low-level cyclonic circulation favoring TC development.

The El Niño in autumn 2023 also exhibited some non-canonical spatial characteristics with positive SSTAs over the extratropical western-to-central North Pacific (Fig. 2e). These SSTAs were unlike the classical El Niño SSTA pattern (Fig. 1c). The SSTAs in autumn 2023 showed a structure similar to a warm phase of the North Pacific Mode (NPM; Fig. 1d). Previous studies have considered the NPM to be a significant ENSO-independent North Pacific SSTA mode on interannual timescales (Deser and Blackmon 1995; Zhang et al. 1996; Zhou et al. 2002; An and Wang 2005; Park et al. 2012; Hartmann 2015; Tao et al. 2022). During a warm NPM, midlatitude positive SSTAs are associated with an anomalous large-scale anticyclonic circulation over the North Pacific, corresponding to a weakened Aleutian Low (Park et al. 2012; Hartmann 2015). Given the high correlation between the Aleutian Low index and WNP TC frequency as reported in Choi and Cha (2017), the NPM is likely to impact WNP TC genesis. The objective of this work is to find the primary factors responsible for the record-low WNP TC frequency in autumn 2023 as well as its related physical mechanisms.

Data and methods

WNP TC best track data from 1951 to 2023 are taken from the Regional Specialized Meteorological Center Tokyo—Typhoon Center of the Japan Meteorological Agency. TC genesis is defined as the first record when a TC reaches tropical storm intensity (maximum sustained wind $\geq$ 34 kt). Consistent with Fudeyasu et al. (2018), TCs that formed over the eastern North Pacific and then entered the WNP are excluded. TC genesis frequency (TCGF) is first obtained by counting TC genesis over a $5^{\circ} \times 5^{\circ}$ grid and is then spatially smoothed using the method detailed in Kim et al. (2011).

Monthly mean SST data on a $1^{\circ} \times 1^{\circ}$ grid are obtained from the Hadley Centre Sea Ice and Sea Surface Temperature data set (HadISST; Rayner et al. 2003). The ENSO Modoki index (EMI; Ashok et al. 2007) and the mean SSTAs over the Niño-3 region, the midlatitude western-to-central North Pacific (35°–45°N, 140°E–170°W), the western equatorial Indian Ocean (WEIO; 10°S–10°N, 50°–70°E) and the tropical North Atlantic (TNA; 0°–20°N, 80°–25°W) are all calculated from detrended SST fields. The Pacific Meridional Mode (PMM) index is downloaded from the Physical Sciences Laboratory of the National Oceanic and Atmospheric Administration. Monthly mean atmospheric variables on a $0.25^{\circ} \times 0.25^{\circ}$ grid are taken from the fifth generation European Centre for Medium-Range Weather Forecasts reanalysis of the global climate (ERA5; Hersbach et al. 2020). Oceanic and atmospheric variables in the HadISST and ERA5 datasets are used to calculate two versions of the genesis potential index (GPI): the GPI developed by Emanuel and Nolan (2004; ENGPI) and the dynamic GPI (DGPI) developed by Wang and Murakami (2020). ENGPI consists of both thermodynamic and dynamic variables: maximum potential intensity (MPI), 700–500-hPa relative humidity, 850-hPa absolute vorticity and 850–200-hPa vertical wind shear (VWS). By comparison, the DGPI consists of four dynamic variables: 850–200-hPa VWS, 850-hPa absolute vorticity, 500-hPa vertical velocity and the meridional gradient of the 500-hPa zonal wind. Greater GPIs typically correspond to increased TC genesis frequency, resulting from positive anomalies of MPI, relative humidity and absolute vorticity and negative anomalies of VWS, vertical velocity and the zonal wind meridional gradient.

The significance levels (p) of correlation coefficients (r) and linear regressions are both estimated by using a two-tailed Student's t-test. When evaluating statistical significance, the effective sample size proposed by Trenberth (1984) is applied to minimize the influence of autocorrelations.

The leading modes of interannual variability in SSTAs are derived from an empirical orthogonal function (EOF) analysis. The EOF decomposition is performed on monthly SSTAs over the tropical and North Pacific (20°S–60°N, 120°E–80°W), following Zhang et al. (1996) and An and Wang (2005). The leading three EOFs resemble the patterns of El Niño with positive SSTAs over the equatorial central-to-eastern Pacific (Fig. 1c), El Niño Modoki/positive PMM with positive SSTAs extending from the subtropical northeastern Pacific to the equatorial central Pacific (Figure S3 in the supplementary information), and a warm NPM with positive SSTAs over the midlatitude western-to-central North Pacific (Fig. 1d). Hereafter, we consider the first and third principal components (PCs) as the ENSO and NPM indices, respectively.

Results and discussion

Seasonal evolution of the large-scale environment from autumn 2022 to autumn 2023

Positive SSTAs began to appear over the midlatitude western-to-central North Pacific in autumn 2022. These positive SSTAs are a typical feature for a developing La Niña (Fig. 2a). This pattern persisted in winter 2022/23, with no obvious changes in either the WEIO or the TNA (Fig. 2b). In spring 2023, the La Niña decayed, while El Niño developed with the highest SSTAs over the coastal eastern Pacific (Fig. 2c). Positive SSTAs also occurred over the Niño-3 region and the WEIO, while TNA SSTAs were weak. SSTAs remained positive over the midlatitude western-to-central North Pacific, which is atypical for the canonical El Niño SSTA structure across the North Pacific.

A similar SSTA pattern prevailed during the summer and autumn, with warmer SSTAs over the Niño-3 region, the WEIO, and the TNA as well as the midlatitude western-to-central North Pacific (Fig. 2d, e). There is a significant simultaneous correlation between Niño-3 SSTA with SSTAs over the WEIO and the TNA during 1951–2023, with correlations of 0.68 ($p < 0.01$) and 0.24 ($p = 0.04$), respectively. Also as shown in Fig. 2a–e, the three regions (Niño-3 region, WEIO and TNA) started to warm at almost the same time. This result implies that the positive SSTAs over the WEIO and the TNA in autumn 2023 were very likely the result of the developing El Niño. By contrast, compared with other strong El Niños (Figure S2 in the supplementary information), El Niño in 2023 had much warmer SSTAs over the midlatitude western-to-central North Pacific (Fig. 2c–e). This is atypical for El Niño events, as there is an inverse relationship between SSTAs over the Niño-3 region and the midlatitude western-to-central North Pacific during 1951–2023 ($r = -0.36$; $p < 0.01$). Therefore, although several publications have reported a remote influence of SSTAs over the Indian Ocean and the Atlantic on WNP TC activity (e.g., Du et al. 2011; Yu et al. 2016), this study focuses on the impact of Pacific SSTAs.

In addition, the autumn 2023 value of the PMM was quite negative—the lowest since 1997. When focusing on all three months comprising autumn (September–November), Fu et al. (2023) reported a significant positive correlation between WNP TC number and the PMM. However, in autumn 2023, the SSTA pattern was not structured like a typical negative PMM pattern (Fig. 2e). Negative SSTAs weakened over the subtropical northeastern Pacific, while positive SSTAs extended from the equatorial eastern Pacific to the equatorial central Pacific. Owing to the lack of similarity in the spatial SSTA pattern between autumn 2023 and the canonical PMM, we do not believe that the PMM played a significant role in modulating autumn 2023 TC activity.

Accompanied by the peak SSTA increases over the midlatitude western-to-central North Pacific, there were ocean fronts with notable SSTA gradients (Fig. 2a–e). Small et al. (2008) showed that a positive correlation between SST and surface wind speed indicated that the ocean was forcing the atmosphere, while a negative correlation suggested that the atmosphere was driving the ocean. Figure 2f–o displays seasonal changes in sea level pressure and 10-m wind. Over the Aleutian Low region (30°–65°N, 160°E–140°W), an anomalous high was observed from autumn 2022 to spring 2023 (Fig. 2f–h). Associated with this anomalous surface high were decreased surface wind speeds, because the anomalous surface easterlies counteracted the climatological surface westerlies (Fig. 2k–m). This implies that atmospheric changes (e.g., a weakened Aleutian Low) drove the warming of the midlatitude western-to-central North Pacific.

By comparison, beginning in summer 2023, increased surface wind speeds and anomalous surface westerlies occurred over the Aleutian Low region (Fig. 2n, o). Associated with this circulation was a dipole in surface pressure, with an anomalous surface low to the north and an anomalous surface high to the south (Fig. 2i, j). As noted in Small et al. (2008), this surface pressure pattern was likely forced by the anomalously warm midlatitude western-to-central North Pacific.

Changes in WNP TC genesis modulated by the ENSO and the NPM

Figure 1a, b shows the annual variation of WNP TC frequency in boreal autumn from 1951 to 2023. Only four TCs (Yun-Yeung, Koinu, Bolaven, and Sanba) formed over the WNP in autumn 2023, the fewest on record and well below the climatological average of 11 TCs. Given that autumn WNP TC frequency has decreased at a weak and insignificant rate ($-$ 0.02 TCs yr^{-1}; $p = 0.17$) during 1951–2023, the long-term trend likely played a minimal role in the record-low value observed in 2023.

Figure 1a also shows a weak inverse relationship between autumn WNP TC frequency and the simultaneous ENSO index during 1951–2023 ($r = -0.22$; $p = 0.06$), consistent with Choi et al. (2019). A strong El Niño was developing in autumn 2023, with the sixth largest Niño-3 SSTA (1.7℃) during the 73-year period. By contrast, the five strongest El Niños since 1951 had TC numbers close to the climatological average of 11 TCs (Figure S2 in the supplementary information). 1972 had 12 TCs, 1982 had 9 TCs, 1987 had 10 TCs, 1997 had 9 TCs and 2015 had 10 TCs. This weak relationship between El Niño and autumn WNP TC frequency highlights that the record-low TC frequency in autumn 2023 was not solely induced by the strong El Niño.

There is a significant negative correlation between WNP autumn TC frequency and the concurrent NPM index during 1951–2023 ($r = -0.37$; $p < 0.01$; Fig. 1b). Of note is that autumn 2023 had the highest NPM index during the 73-year period. When removing the influence of the midlatitude western-to-central North Pacific SSTA, the partial correlation between TC frequency and the NPM index becomes insignificant ($r = -0.11$; $p = 0.38$). By contrast, the partial correlation is nearly unchanged ($r = -0.37$; $p < 0.01$) if the influence of the Niño-3 SSTA is removed. This suggests that the impact of the NPM on WNP TC frequency is mainly due to SSTA changes over the midlatitude western-to-central North Pacific. A coherence spectrum analysis further shows that correlations of autumn WNP frequency with the ENSO and NPM indices primarily occur at interannual timescales ranging from 2 to 4 years, with no significant relationship found at longer timescales (figure not shown).

Positive SSTAs were concentrated over two zonal belts in autumn 2023 (Fig. 2e). The positive SSTAs over the equatorial central-to-eastern Pacific were much larger (smaller) than those over the midlatitude western-to-central North Pacific. When reconstructing SSTAs using the first and third EOFs and their corresponding PCs, the reconstructed SSTAs in 2023 showed an extremely high similarity to observed SSTAs (Fig. 1e), with a pattern correlation of 0.94 ($p<0.01$). This confirms that El Niño and a warm NPM were the primary climate modes driving the observed Pacific SSTAs in autumn 2023.

We also performed an EOF decomposition on gridded autumn TCGFs during 1951–2023. The first EOF displays a basinwide change in WNP TCGFs (Fig. 1f), while the second EOF displays an east–west dipolar pattern in TCGF changes (Fig. 1 g). Furthermore, as shown in Fig. 1a, b, the first TCGF PC is significantly anti-correlated with the NPM ($r=-\ 0.33$; $p<0.01$), while the second TCGF PC is significantly correlated with ENSO ($r=0.42$; $p<0.01$). This means that changes in the leading TCGF patterns are significantly linked to phase changes in ENSO and the NPM.

Figure 3a and b displays the spatial distributions of TCGFs regressed onto the ENSO and NPM indices, respectively. Given that the ENSO and PMM indices are both derived from EOF analyses, their influences on TC genesis are linearly independent. Consistent with numerous previous publications (e.g., Lander 1994; Chan 1985, 2000; Saunders et al. 2000; Wang and Chan 2002; Camargo et al. 2007), during an El Niño, TC genesis is significantly enhanced (suppressed) over the southeastern (northwestern) part of the WNP (Fig. 3a). By comparison, during a warm NPM, TC genesis is suppressed over most of the WNP, except for the northwestern SCS (Fig. 3b). Significant TCGF reductions are concentrated over a region spanning 10°–20°N and 140°–160°E, which is slightly east of the region with significant Aleutian Low-induced TCGF changes (10°–20°N, 130°–155°E; Choi and Cha 2017).

TCGF anomalies can be further calculated as a linear sum of the regressions of TCGF multiplied by the ENSO and NPM indices. In 2023, TC genesis was estimated to decrease west of 140°E (Fig. 3c), due to both El Niño-induced and warm NPM-induced TC genesis suppressions. Over the region spanning 140°E–160°E, the regressions of TCGFs onto the ENSO and NPM indices are of comparable magnitudes but are of opposite signs (Fig. 3a, b). Given that the NPM index was relatively higher than the ENSO index in autumn 2023 (Fig. 1a, b), the TC-suppressing effect of the warm NPM tended to dominate over the TC-enhancing effect of El Niño in that region, leading to decreases in estimated TCGF (Fig. 3c). There were estimated increases in TCGF east of 160°E (Fig. 3c), due to significantly enhanced TCGF induced by El Niño and nearly unchanged TCGF induced by the warm NPM.

In autumn 2023, most of the observed TCGF decreases occurred over 10°–20°N and 110°–160°E (Fig. 3d). This observed distribution is similar to the reconstructed TCGFs, with a pattern correlation of 0.79 ($p<0.01$). The reconstructed TCGF is derived from the first and second EOFs and their corresponding PCs (Fig. 1 h). Over most of the WNP, the observed TCGF reductions are well captured by the TCGF anomalies estimated by the ENSO and NPM indices, which highlights that TC genesis changes in 2023 were primarily linked to El Niño and a warm NPM. By comparison, the TCGFs east of 160°E and south of 20°N were suppressed in observations but were estimated to be enhanced based on the ENSO and NPM indices. These observed TCGF decreases were likely induced by other factors (e.g., a negative North Pacific Oscillation phase) in autumn 2023. In addition, climatologically, there are 0.6 autumn TCs forming east of 160°E and south of 20°N, accounting for only 5% of WNP TCs (Figure S5 in the supplementary information). When focusing on El Niño events, there are, on average, 1.1 autumn TCs forming over this region, accounting for 11% of WNP TCs (Figure S6 in the supplementary information). The autumn TC frequency in 2023 was 4, which is 2 TCs fewer than in the second lowest year (6 autumn TCs in 2010). Even if the canonical ENSO and NPM index relationship with TCGF increases east of 160°E had held in autumn 2023, basinwide TC frequency would likely have remained at its historical lowest level.

Changes in environmental conditions as modulated by ENSO and the NPM

Figure 3e–h and Fig. 3i–l display spatial changes in the DGPI and ENGPI, respectively. The results using the GPI broadly show good consistency with those for TCGF, regardless of which GPI is considered. During an El Niño, GPIs are significantly enhanced (suppressed) over the southeastern (northwestern) portion of the WNP (Fig. 3e, i). During a warm NPM, significantly decreased GPIs occur over 10°–20°N and 130°–160°E. This region extends more eastward and covers a larger area than the region with significantly decreased TCGF (Fig. 3f, j). There are decreases in both estimated and observed GPI anomalies in 2023 over a zonal belt spanning 10°–20°N (Fig. 3 g, h, k, l). These results mean that TC genesis

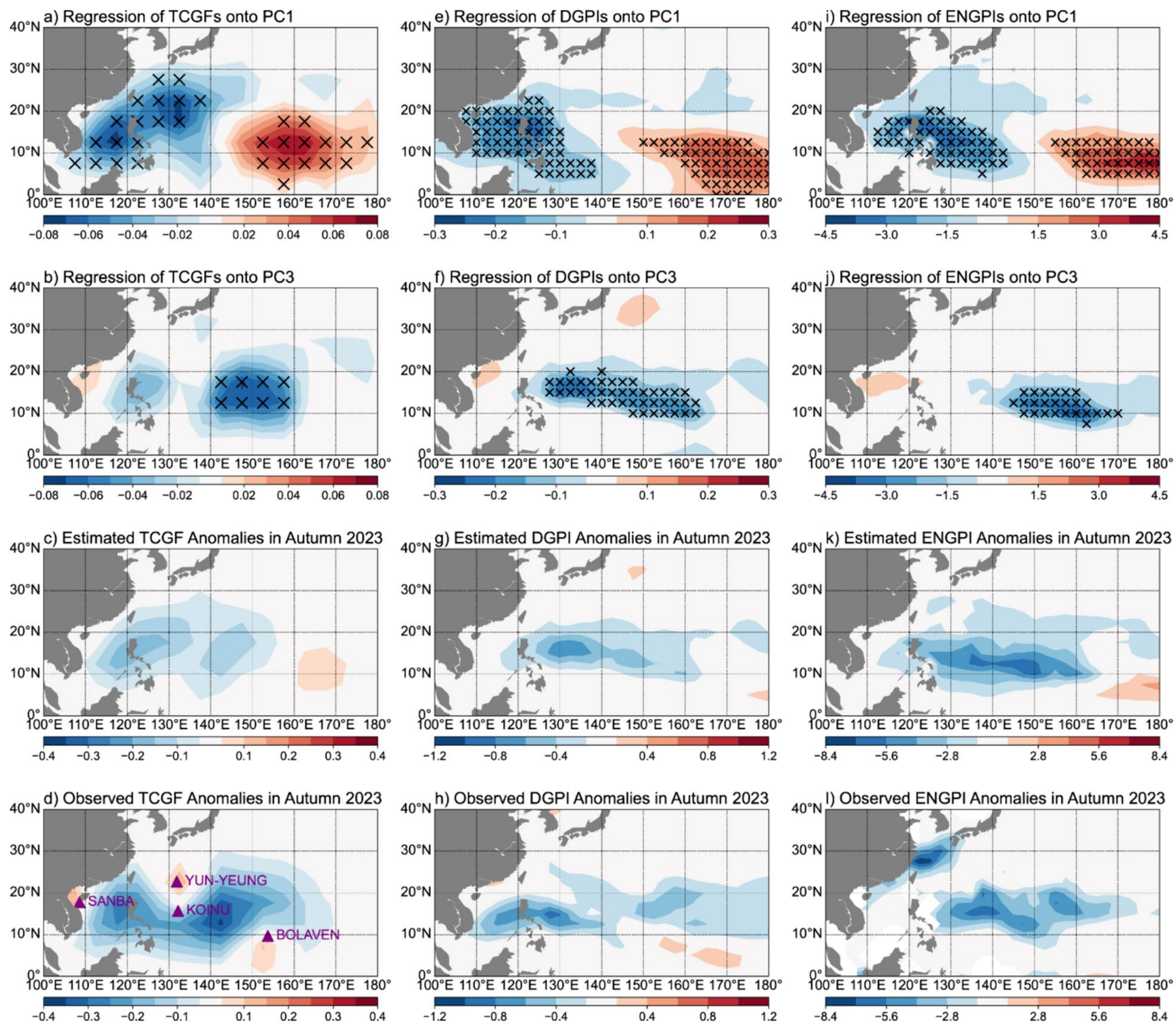

Fig. 3 **a**, **b** Regressions of TCGFs onto the a ENSO and b NPM indices from 1951 to 2023. Black crosses denote regressions significant at the 0.05 level. **c** Estimated TCGF anomalies in autumn 2023 based on the regressions in a and b multiplied by their corresponding indices. **d** Observed TCGF anomalies in autumn 2023. The genesis locations of the four TCs in autumn 2023 are marked with purple triangles. **e**–**h** As in **a**–**d**, but for DGPI. **i**–**l** As in **a**–**d**, but for ENGPI

anomalies in 2023 can be explained by changes in large-scale atmospheric conditions.

During El Niño, significantly enhanced DGPIs and ENGPIs east of 145°E are mainly linked to decreases in 850–200-hPa VWS and increases in 850-hPa relative vorticity and MPI, while significantly reduced DGPIs and ENGPIs west of 145°E are caused by increases in the meridional gradient of the zonal wind and vertical velocity at 500 hPa, along with decreases in 850-hPa relative vorticity, MPI and 700–500-hPa relative humidity (Figure S4 in the supplementary information). Given previous extensive research on the ENSO–WNP TC relationship (e.g., Lander 1994; Chan 1985, 2000; Saunders et al. 2000; Wang and Chan 2002; Camargo et al. 2007), we only highlight here that relative vorticity tends to be the most important contributor to the DGPI and ENGPI by ENSO over both the eastern and western parts of the WNP.

During a warm NPM, over the region with significant TCGF changes (10°–20°N, 140°–160°E), there are significant increases in 850–200-hPa VWS, 500-hPa vertical velocity and 700–500-hPa relative humidity and significant decreases in 850-hPa relative vorticity. There are only weak changes in the 500-hPa meridional gradient of the zonal wind and MPI (Fig. 4a–e). Note that the impact of relative humidity changes is opposite to those of the other significantly changed factors. When focusing on

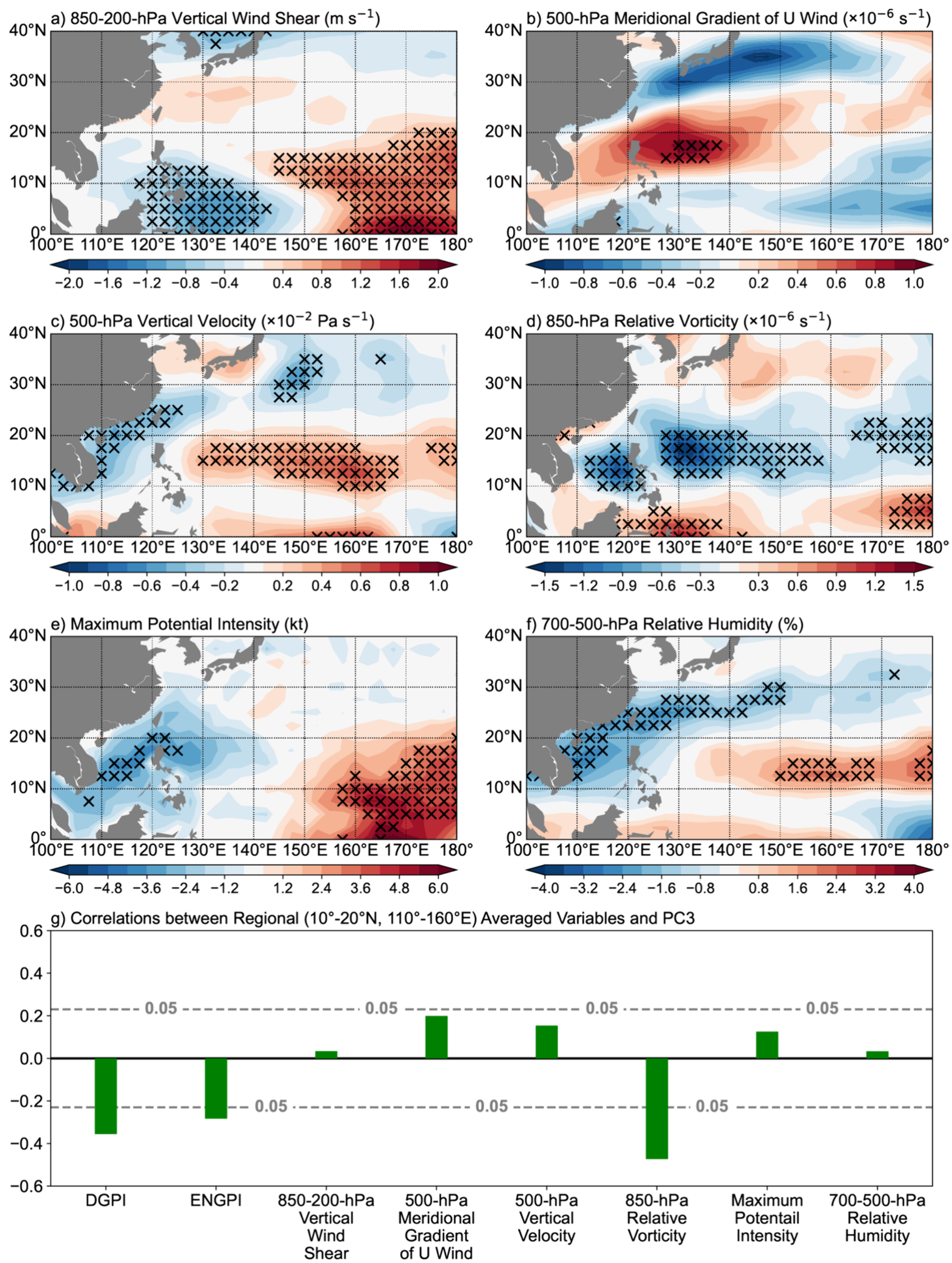

Fig. 4 **a**–**d** Regressions of **a** 850–200-hPa VWS, **b** 500-hPa meridional gradient of zonal wind, **c** 500-hPa vertical velocity, **d** 850-hPa relative vorticity, **e** MPI and **f** 700–500-hPa relative humidity onto the NPM index during 1951–2023. **g** Correlations between regionally averaged (10°–20°N, 110°–160°E) environmental variables and the NPM index. Dashed lines denote statistical significance at the 0.05 level

the region with the highest climatological TC formation (10°–20°N, 110°–160°E; Figure S5 in the supplementary information), relative vorticity is the dominant factor determining NPM's effect on both the DGPI and the ENGPI (Fig. 3 g). This is because significant changes in VWS, vertical velocity and relative humidity only occur over the eastern part of the highest TC forming region (east of 145°E, 130°E and 150°E, respectively), while significant decreases in relative vorticity span from 110°E to the dateline. Due to the dominant role of relative vorticity, the DGPI and ENGPI changes exhibit similar distributions as displayed in Fig. 3e–l.

The change in relative vorticity are directly linked to an anomalous low-level WNP circulation. During El Niño, there are significant anomalous westerlies at 850 hPa over the equatorial Pacific, associated with a large-scale anomalous anticyclone centered over the SCS, along with a large-scale anomalous cyclone centered near 40°N, 160°W (Fig. 5a). This flow pattern is consistent with composite wind anomalies during eastern Pacific El Niños as reported in Kim et al. (2011). The anomalous anticyclone spans the western WNP, resulting in negative vorticity anomalies. There is a trough extending southwestward from the anomalous cyclone's center to the eastern WNP, producing positive vorticity anomalies. By comparison, during a warm NPM, there is a large-scale anomalous low-level anticyclonic circulation centered near 40°N, 180°, with significant flow anomalies mainly occurring in the midlatitudes (Fig. 5b). This feature is also shown in Park et al. (2012) and Tao et al. (2022), corresponding to a weakened Aleutian Low. Most of the WNP is in the southwestern quadrant of this anomalous anticyclone, where negative vorticity anomalies predominate.

The 850-hPa anomalous flow in autumn 2023, estimated by summing the regressions of the flow multiplied by the ENSO and NPM indices, is complex (Fig. 5c). South of 20°N, the anomalous flow has a similar structure to the El Niño-induced flow, possibly because of a strong (weak) response of the low-level flow to ENSO (NPM). Anomalous westerlies extend from the western Pacific to the eastern Pacific, along with an anomalous SCS anticyclone that suppresses TC genesis over the western WNP. North of 20°N, there is an anomalous anticyclone centered near 40°N, 160°E, which is near the location of the warm NPM-induced anticyclone shown in Fig. 5b. This result implies that this anomalous anticyclone is primarily linked to positive SSTAs over the midlatitude western-to-central North Pacific. The warm NPM-induced midlatitude anticyclone causes shifts in the observed circulation pattern compared with the El Niño-induced flow displayed in Fig. 5a, with the anomalous cyclone shifted southeastward into the subtropical northeastern Pacific

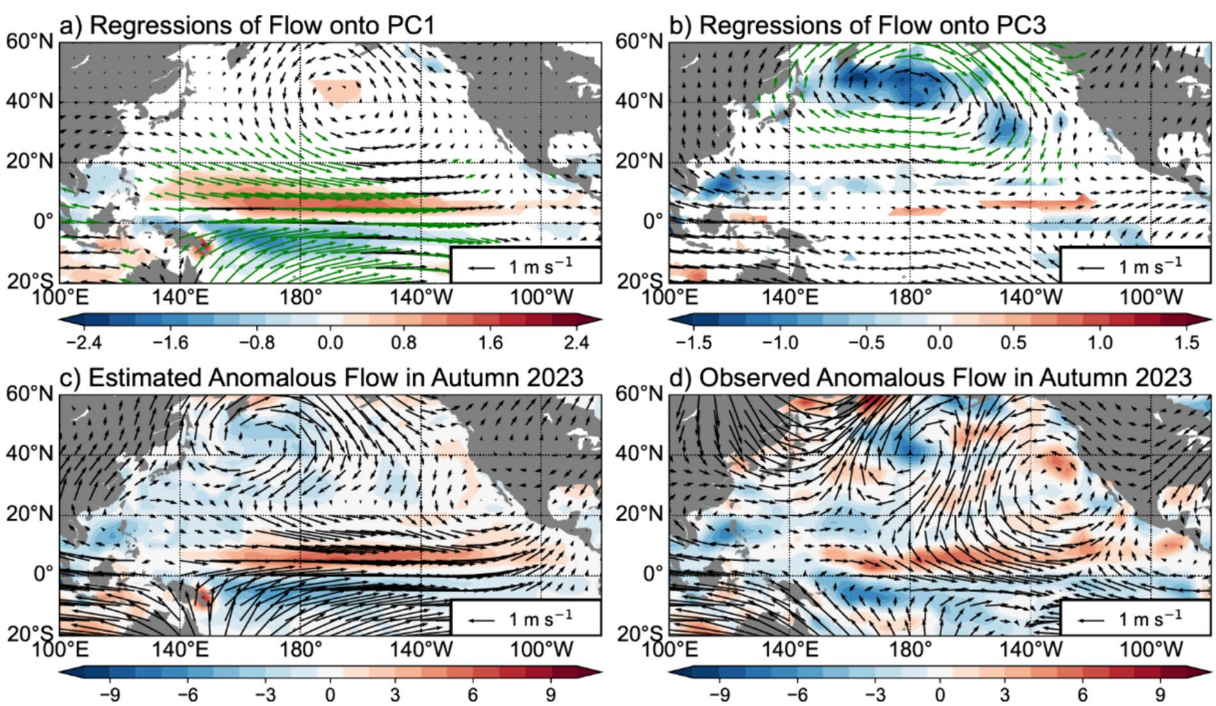

Fig. 5 **a**, **b** Regressions of 850-hP a horizontal wind vectors and relative vorticity onto **a** ENSO and **b** the NPM indices from 1951 to 2023. Green vectors denote flow anomalies significant at the 0.05 level. Only regressions of relative vorticity significant at the 0.05 level are shown. **c** Estimated 850-hPa anomalous wind vectors and relative vorticity anomalies in autumn 2023 based on the regressions in **a** and **b** multiplied by their corresponding indices. **d** Observed 850-hPa anomalous wind vectors and relative vorticity anomalies in autumn 2023

(Fig. 5c–d). Over the subtropical eastern WNP, there is a warm NPM-induced anticyclonic circulation instead of an eastward-retreated ENSO-induced cyclonic circulation, reducing TC genesis.

In addition, the estimated 850-hPa anomalous flow captures the general characteristics of the observed flow in autumn 2023 (Fig. 5d). One difference is that compared with observations, the estimated anomalous anticyclone over the North Pacific shifts eastward, and the estimated anomalous cyclone over the northeastern Pacific shifts westward (Fig. 5c, d). Another difference is that there is an observed wave train-like pattern with anomalous northerlies around the dateline (Fig. 5d). This pattern does not occur in the estimated anomalous flow (Fig. 5c). Although the general pattern of the anomalous low-level flow in autumn 2023 can be attributed to the linear combination of El Niño and a warm NPM, there are other climate modes influencing the low-level circulation over some portions of the WNP in autumn 2023.

Conclusions

Autumn 2023 had the fewest WNP TCs during autumn since 1951. This period was associated with a strong El Niño and a warm NPM. There is only a weak inverse relationship between autumn WNP TC frequency during autumn and the simultaneous ENSO index from 1951 to 2023, likely due to the northwest–southeast dipolar change in TC genesis caused by ENSO. By contrast, TC frequency is significantly anti-correlated with the NPM index. Reduced TC genesis occurs over most of the WNP during a warm NPM, with significant TCGF decreases occurring over the region spanning 10°–20°N, 140°–160°E. When focusing on autumn 2023, decreases in TC genesis west of 140°E were jointly linked to El Niño-induced and warm NPM-induced reductions in TCGF. By comparison, decreases in TC genesis over the region spanning 140°E–160°E were caused by the TC-suppressing effect of the warm NPM tending to exceed the TC-enhancing effect of El Niño.

Given that the changes in both the DGPI and ENGPI show good consistency with changes in TCGF, the influences of ENSO and the NPM on TC genesis can be explained by environmental changes. During El Niño, there are significant decreases in 850–200-hPa VWS and significant increases in 850-hPa relative vorticity east of 145°E. There are significant increases in the meridional gradient of the zonal wind and vertical velocity at 500 hPa and significant decreases in 850-hPa relative vorticity, MPI and 700–500-hPa relative humidity west of 145°E. During a warm NPM, there are significant increases in 850–200-hPa VWS and 500-hPa vertical velocity and significant decreases in 850-hPa relative vorticity over 10°–20°N and 140°–160°E. These results indicate that relative vorticity tends to be the most important factor for comparing the influences of ENSO and the NPM on WNP TC genesis.

The anomalous low-level flow in autumn 2023 exhibited a combination of the response to an El Niño and a warm NPM. South of 20°N, the anomalous flow was mainly influenced by El Niño, with an anomalous anticyclone over the SCS that suppressed TC genesis over the western WNP. North of 20°N, there was an anomalous anticyclone centered at around 40°N, 160°E—a typical feature during a warm NPM. This resulted in an anticyclonic circulation reducing TC genesis over the western WNP, instead of just the eastward retreat in TC-favoring conditions generated by the ENSO-induced cyclonic circulation.

By analyzing the sole and joint influences of the ENSO and the NPM on WNP TC genesis, this study highlights that the record-low TC activity in autumn 2023 was likely driven by the co-occurrence of El Niño and a warm NPM. In autumn 2023, there were two zonal belts of positive SSTAs. The first zonal belt was located over the equatorial central-to-eastern Pacific, while the second was located over the midlatitude western-to-central North Pacific. This spatial SSTA structure has not been observed in the developing phase of other historically strong El Niños (e.g., 1972, 1982, 1987, 1997 and 2015).

As displayed in Fig. 2d, there was also a combined pattern of El Niño and a warm NPM in summer 2023. However, consistent with the weak correlations of summer WNP TC frequency versus the simultaneous ENSO index ($r = -0.05$; $p = 0.66$) and the simultaneous NPM index ($r = -0.10$; $p = 0.30$), WNP TC activity in summer 2023 was close to its long-term average. 10 WNP TCs formed in summer 2023, which is near the climatological (1951–2023) average of 11.1. This result further implies that a specified climate mode (e.g., ENSO, NPM, etc.) can pose different impacts on basinwide WNP TC activity during different seasons, as noted in previous publications (e.g., Choi et al. 2019; Fu et al. 2023).

Xu et al. (2021) reported that during recent decades, SST warming trends over the extratropical North Pacific were higher than for other Pacific sub-regions, implying an increasing probability of a warm NPM. This warming trend may play a considerable role in projected decreases in WNP TCs. Our main findings will be verified in future work using numerical experiments and different SSTA forcings over the tropical and North Pacific.

Supplementary Information

The online version contains supplementary material available at https://doi.org/10.1186/s40562-024-00350-w.

Supplementary Material 1.

Acknowledgements

The authors would like to express their sincere thanks to two anonymous reviewers and the editor for their helpful comments on an earlier version of this manuscript. The authors appreciate the provision of computing resources and support by the Jiangsu Meteorological Bureau of China.

Author contributions

JS proposed the subject of this paper and wrote the manuscript. PJK and YD revised the manuscript. JS and NW contributed to data collection and statistical analysis. All authors read and approved the final manuscript.

Funding

This work was jointly funded by the National Natural Science Foundation of China (U2342203, 42192554, 61827901, 42175007 and 42305005), the Meteorological Research Program of Guangxi Province of China (2023ZL04), and the G. Unger Vetlesen Foundation.

Availability of data and materials

HadISST data were downloaded from the Hadley Centre for Climate Prediction and Research/Met Office/Ministry of Defence/United Kingdom at: https://doi.org/https://doi.org/10.5065/XMYE-AN84. ERA5 data were retrieved from the Copernicus Climate Change Service Data at: https://doi.org/https://doi.org/10.24381/cds.143582cf. Monthly values of the PMM index were obtained from: https://psl.noaa.gov/data/timeseries/monthly/PMM/. Monthly values of the AMM were obtained from: https://psl.noaa.gov/data/timeseries/monthly/AMM/. TC best track data are available at: https://www.jma.go.jp/jma/jma-eng/jma-center/rsmc-hp-pub-eg/trackarchives.html.

Declarations

Competing interests

The authors declare that they have no competing interests.

Received: 1 April 2024 Accepted: 27 July 2024
Published online: 08 August 2024

References

An S, Wang B (2005) The forced and intrinsic low-frequency modes in the North Pacific. J Clim 18:876–885

Ashok K, Behera SK, Rao SA, Weng H, Yamagata T (2007) El Niño Modoki and its possible teleconnections. J Geophys Res 112:C11007

Basconcillo J, Cha E-J, Moon I-J (2021) Characterizing the highest tropical cyclone frequency in the western North Pacific since 1984. Sci Rep 11:14350

Camargo SJ, Emanuel KA, Sobel AH (2007) Use of a genesis potential index to diagnose ENSO effects on tropical cyclone genesis. J Clim 20:4819–4834

Chan JCL (1985) Tropical cyclone activity in the northwest Pacific in relation to the El Niño/Southern Oscillation phenomenon. Mon Weather Rev 113:599–606

Chan JCL (2000) Tropical cyclone activity over the western North Pacific associated with El Niño and La Niña events. J Clim 13:2960–2972

Choi J, Cha Y (2017) Anomalous variation in summer tropical cyclone activity by preceding winter Aleutian low oscillation. Atmos Sci Lett 18:268–275

Choi Y, Ha K, Jin F (2019) Seasonality and El Niño diversity in the relationship between ENSO and western North Pacific tropical cyclone activity. J Clim 32:8021–8045

Deser C, Blackmon ML (1995) On the relationship between tropical and North Pacific sea surface temperature variations. J Clim 8:1677–1680

Du Y, Yang L, Xie SP (2011) Tropical Indian Ocean influence on Northwest Pacific tropical cyclones in summer following strong El Niño. J Clim 24:315–322

Emanuel KA (2018) 100 years of progress in tropical cyclone research. Meteorol Monogr 59:15.1-15.68

Emanuel KA, Nolan D. Tropical cyclone activity and the global climate system, preprints, 26th Conference on Hurricanes and Tropical Meteorology, Miami, Fla., Am. Meteor. Soc. A. 2004.

Fu M, Wang C, Wu L, Zhao H (2023) Season-dependent modulation of Pacific Meridional Mode on tropical cyclone genesis over the western North Pacific. J Geophys Res 128:e2022JD037575

Fudeyasu H, Ito K, Miyamoto Y (2018) Characteristics of tropical cyclone rapid intensification over the western North Pacific. J Clim 31:8917–8930

Gao S, Zhu L, Zhang W, Shen X (2020) Western North Pacific tropical cyclone activity in 2018: a season of extremes. Sci Rep 10:5610

Hartmann DL (2015) Pacific sea surface temperature and the winter of 2014. Geophys Res Lett 42:1894–1902

Hersbach H, Bell B, Berrisford P, Hirahara S, Horanyi A, Muñoz-Sabater J, Nicolas J, Peubey C, Radu R, Schepers D, Simmons A, Soci C, Abdalla S, Abellan X, Balsamo G, Bechtold P, Biavati G, Bidlot J, Bonavita M, Chiara G, Dahlgren P, Dee D, Diamantakis M, Dragani R, Flemming J, Forbes R, Fuentes M, Geer A, Haimberger L, Healy S, Hogan RJ, Holm E, Janiskova M, Keeley S, Laloyaux P, Lopez P, Lupu C, Radnoti G, Rosnay P, Rozum I, Vamborg F, Villaume S, Thépaut J (2020) The ERA5 global reanalysis. Q J R Meteorol Soc 146:1999–2049

Hu P, Huangfu J, Chen W, Huang R (2020) Impacts of early/late South China Sea summer monsoon withdrawal on tropical cyclone genesis over the western North Pacific. Clim Dyn 55:1507–1520

Kim H, Webster PJ, Curry JA (2011) Modulation of North Pacific tropical cyclone activity by three phases of ENSO. J Clim 24:1839–1849

Lander MA (1994) An exploratory analysis of the relationship between tropical storm formation in the western North Pacific and ENSO. Mon Weather Rev 122:636–651

Lee T-C, Knutson TR, Kamahori H, Ying M (2012) Impacts of climate change on tropical cyclones in the western North Pacific basin. Part I: past observations. Trop Cycl Res Rev 1:213–230

Liu C, Zhang W, Jiang F, Stuecker MF, Huang Z (2021) Record-low WNP tropical cyclone activity in early summer 2020 due to Indian Ocean warming and Madden–Julian Oscillation activity. Geophys Res Lett 48:e2021GL094578

Maue RN (2011) Recent historically low global tropical cyclone activity. Geophys Res Lett 38:L14803

Park J-Y, Yeh S-W, Kug J-S (2012) Revisited relationship between tropical and North Pacific Sea surface temperature variations. Geophys Res Lett 39:L02703

Rayner NA, Parker DE, Horton EB, Folland CK, Alexander LV, Rowell DP, Kent EC, Kaplan A (2003) Global analyses of sea surface temperature, sea ice, and night marine air temperature since the late nineteenth century. J Geophys Res 108:4407

Saunders MA, Chandler RE, Merchant CJ, Roberts FP (2000) Atlantic hurricanes and NW Pacific typhoons: ENSO spatial impacts on occurrence and landfall. Geophys Res Lett 27:1147–1150

Small R, Szoeke D, Xie SP, O'Neill L, Seo H, Song Q, Cornillon P, Spall M, Minobe S (2008) Air–sea interaction over ocean fronts and eddies. Dyn Atmos Oceans 45:274–319

Tao L, Fang J, Yang X-Q, Sun X, Cai D (2022) Midwinter reversal of the atmospheric anomalies caused by the North Pacific Mode-related air–sea coupling. Geophys Res Lett 49:e2022GL100307

Trenberth KE (1984) Some effects of finite sample size and persistence on meteorological statistics. Part I: Autocorrelations. Monthly Weather Rev 112:2359–2368

Wang B, Chan JCL (2002) How strong ENSO events affect tropical storm activity over the western North Pacific. J Clim 15:1643–1658

Wang B, Murakami H (2020) Dynamic genesis potential index for diagnosing present-day and future global tropical cyclone genesis. Environ Res Lett 15:114008

Wang C, Wu K, Wu L, Zhao H, Cao J (2021) What caused the unprecedented absence of western North Pacific tropical cyclones in July 2020? Geophys Res Lett 48:e2020GL092282
Xu Z, Ji F, Liu B, Feng T, Gao Y, He Y, Chang F (2021) Long-term evolution of global sea surface temperature trend. Int J Climatol 41:4494–4508
Yao X, Zhao D, Li Y (2020) Autumn tropical cyclones over the western North Pacific during 1949–2016: a statistical study. J Meteorol Res 34:150–162
Yu J, Li T, Tan Z, Zhu Z (2016) Effects of tropical North Atlantic SST on tropical cyclone genesis in the western North Pacific. Clim Dyn 46:865–877
Zhang Y, Wallace JM, Iwasaka N (1996) Is climate variability over the North Pacific a linear response to ENSO? J Clim 9:1468–1478
Zhang P, Wu Z, Zhu Z, Jin R (2022) Promoting seasonal prediction capability of the early autumn tropical cyclone formation frequency over the western North Pacific: effect of Arctic sea ice. Environ Res Lett 17:124012
Zhou T, Yu R, Li Z (2002) ENSO-dependent and ENSO-independent variability over the mid-latitude North Pacific: Observation and air–sea coupled model simulation. Adv Atmos Sci 19:1127–1147

Publisher's Note